UNIVERSITY OF CALIFORNIA SAN DIEGO

Modelling Neuronal Circadian Rhythms in Bipolar Disorder using Human Induced Pluripotent Stem Cells

A thesis submitted in partial satisfaction of the requirements
for the degree Master of Science

in

Biology

by

Noelle Mairi Ying

Committee in charge:

Professor Michael J. McCarthy, Chair
Professor Nicholas Spitzer, Co-Chair
Professor Susan Golden

2020

The thesis of Noelle Mairi Ying is approved, and it is acceptable in quality and form for publication on microfilm and electronically:

_____

_____

Co-Chair

_____

Chair

University of California San Diego

2020

TABLE OF CONTENTS

Signature Page iii

Table of Contents iv

List of Figures v

Abstract of the Thesis vi

Introduction
1.1 Bipolar Disorder 1
1.2 Bipolar Disorder and Lithium 1
1.3 Lithium and the Molecular Circadian Clock 2
1.4 Modelling Bipolar Disorder 4

Materials and Methods
2.1 Human Subjects 8
2.2 hiPSC Culture 9
2.3 Embryoid Body Cell Culture 10
2.4 Neural Rosette Cell Culture 11
2.5 Neural Progenitor Cell Culture 11
2.6 Neuron Cell Culture 12
2.7 Immunocytochemistry 12
2.8 Gene Expression Analysis using Quantitative Polymerase Chain Reaction (qPCR) 13
2.9 Circadian Rhythm Recording: Recording via Luminometer 15
2.10 Single-Cell Recording via Time-Lapse Bioluminescence Microscopy 16
2.11 Data Analysis 16

Results
3.1 Culture of hiPSC-Derived Neurons 18
3.2 Expression of Core Circadian Clock Genes is Increased in Bipolar Disorder NPCs and Neurons 20
3.3 Circadian Rhythm Parameters Differ Between Control, BD Li Responder, and BD Li Non-Responder Cells 23
3.4 Effects of Lithium on Period 27
3.5 Single Cell Analysis Reveals Lower Rhythmicity and Disparate Rhythm Phases in BD NPCs Compared to Control Cells 30
3.6 Temperature Entrainment Rescues Circadian Rhythm Amplitude and Period in BD Neurons 33

Discussion 37

References 42

LIST OF FIGURES

Figure 1.1: The transcriptional-translational negative feedback loop maintains a cell-autonomous 24-hour circadian rhythm 3

Figure 3.1: Patient and control fibroblast-derived hiPSC are differentiated into glutamatergic neurons 19

Figure 3.2: Expression of PER2 and CRY1 is increased in BD NPCs and neurons 22

Figure 3.3: Circadian rhythm amplitude and period differ between Control, BD Responder, and BD Li Non-responder cells 26

Figure 3.4: Lithium mediates concentration-dependent circadian period lengthening in Control and BD Li Responder neurons 29

Figure 3.5: Single cell analysis reveals that BD NPCs are less rhythmic and less phase-aligned compared to Control NPCs 32

Figure 3.6: Temperature entrainment rescues circadian rhythm amplitude and period and lessens rhythm damping in BD neurons 36

ABSTRACT OF THE THESIS

Modelling Neuronal Circadian Rhythms in Bipolar Disorder using Human Induced Pluripotent Stem Cells

by

Noelle Mairi Ying

Master of Science in Biology

University of California San Diego. 2020

Professor Michael J. McCarthy, Chair
Professor Nicholas Spitzer, Co-Chair

Bipolar Disorder (BD) is a lifelong mental disorder characterized by recurrent episodes of mania and depression. Manic episodes involve elevated mood and reduced need for sleep, while depressive episodes are associated with low energy, increased/decreased sleep, and anhedonia. As such, clinical studies have shown that BD patients experience disturbed circadian rhythms. BD is heritable, as is clinical response to the first-line mood stabilizer lithium, suggesting that a biological approach to the etiology of the disorder may provide insight to BD diagnosis and treatment. Previous research in BD patient-derived fibroblasts indicates that circadian rhythm

disturbances extend to the molecular level, but the relationship between BD and the cell-autonomous molecular circadian clock remains to be clarified in the most disease-relevant cell type, neurons.

Using human induced pluripotent stem cell (hiPSC)-derived neural progenitor cells (NPCs) and cortex-like glutamatergic neurons, we measured the oscillatory activity of the molecular circadian clock using a lentiviral *Period2-luciferase* (*Per2-luc*) reporter. We found that BD-associated dysregulation of the molecular clock affects NPCs. In differentiated neurons, BD Li Non-Responder (Li-NR)-derived cells were found to have circadian rhythms not modulated by lithium treatment, and were more phase-dispersed and more resistant to external entrainment factors than were BD Li Responder (Li-R) and healthy control cells. We developed a temperature-entrainment protocol that successfully induced high-amplitude, 24-hour circadian rhythms in neurons from all diagnosis groups, reversing the low-amplitude phenotype in Li-NR neurons. Further characterization of the molecular circadian rhythms of BD hiPSC-derived neurons has the potential to reveal clinically-relevant indicators of BD lithium response.

INTRODUCTION

1.1 Bipolar Disorder

Bipolar Disorder (BD) is a mental disorder characterized by recurrent oscillations between two mood states, mania and depression (McCarthy et al., 2019). Manic episodes are associated with elevated mood, reduced need for sleep, high-risk behavior, and psychosis, while depressive episodes are associated with low mood, low energy, loss of motivation, either increased or decreased sleep, increased or decreased eating, and anhedonia (Beyer and Freund, 2017). BD is estimated to affect 1-2% of the adult population in the U.S. (Clemente et al., 2015) and 15% of patients left untreated commit suicide; BD is therefore recognized as a top global cause of morbidity and lost productivity (O'Shea et al., 2016; Merikangas et al., 2011). Furthermore, BD is 85% heritable, suggesting a considerable biological contribution to the development and symptomology of this disorder and indicating that investigations into the molecular basis of BD are both worthwhile and necessary (McGuffin et al., 2003).

1.2 Bipolar Disorder and Lithium

Treatment for BD involves pharmacotherapy with mood stabilizing medication, accompanied by psychological counseling and anti-depressant medications (Culpepper, 2014). The mood stabilizer lithium, in the form of lithium carbonate, has been used since the 1950s and is considered the "gold standard" of treatment for all phases of BD, including depression, mania, and maintenance therapy (Machado-Vieria et al., 2009). However, lithium is only effective in about 1/3 of BD patients, and the other 2/3 of patients with incomplete or negative responses to lithium therapy must use alternative treatments (McCarthy et al., 2019). Lithium response is a stable, and likely heritable, trait of a given patient's disorder (Grof et al., 2002), but there is

currently no reliable way to predict whether or not a patient will respond clinically to lithium treatment. As such, patients may be prescribed lithium for a trial period of 8-12 weeks before they can be evaluated for symptom remission or exacerbation (McCarthy et al., 2019). However, criteria for drug response may differ across physicians, and patients may have a mixed or incomplete response, may be concurrently using other medications, or may be non-compliant with lithium treatment plans because of side effects such as weight gain and thyroid suppression, further complicating the process of determining lithium response (Oedegaard et al., 2016). This inexact and inefficient trial-and-error process persists because much about lithium's biological mechanism of action remains to be elucidated.

1.3 Lithium and the Molecular Circadian Clock

One known effect of lithium is the inhibition of Glycogen Synthase Kinase 3 (GSK3) (Klein and Melton, 1996). GSK3 has roles within multiple cellular processes, such as cell survival and development, and is a known regulator of the molecular circadian rhythm (Kaladchibachi et al., 2007). Circadian rhythms regulate an organism's sleep/wake, metabolism, and activity cycles, all of which follow a roughly 24-hour repeating pattern (Porcu et al., 2019). In humans, a specialized population of retinal ganglion cells encode information about environmental light and transmit it to a part of the hypothalamus called the suprachiasmatic nucleus (SCN). This influences hormone signaling throughout the body, allowing our circadian rhythms to entrain to a 24-hour light-dark cycle (Porcu et al., 2019).

At the cellular level, each cell maintains a molecular circadian rhythm, the core processes of which can be described as a transcriptional-translational negative feedback loop (Figure 1). The regulatory proteins CLOCK and BMAL1 induce the transcription of *Crytochrome (Cry)* 1 and 2 and *Period homologue (Per)* 1 and 2. *Per* and *Cry* are translated and PER and CRY

accumulate in the cytoplasm before heterodimerizing and re-entering the nucleus to inhibit CLOCK and BMAL1, thereby inhibiting their own transcription. The CRY-PER heterodimer eventually degrades and transcription begins again, creating a 24-hour molecular cycle (Takahashi et al., 2008).

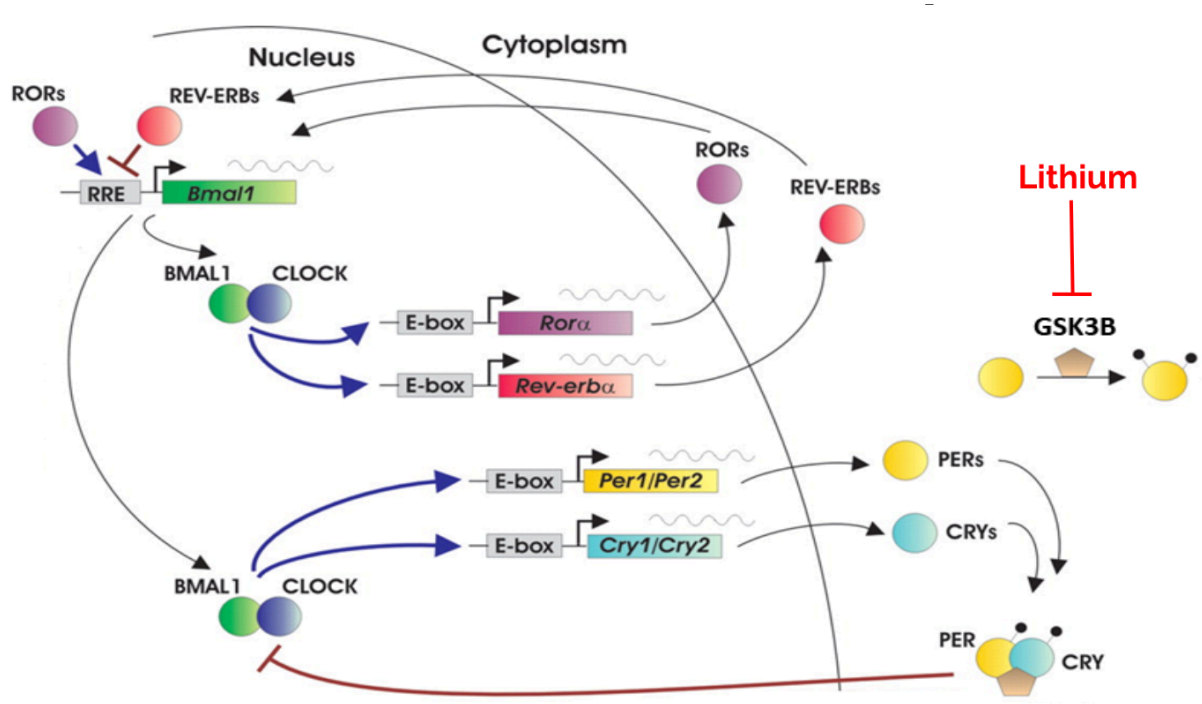

Figure 1.1: The transcriptional-translational negative feedback loop maintains a cell-autonomous 24-hour circadian rhythm. CLOCK and BMAL1 bind to the Enhancer Box (E-Box) region of the *Period* and *Crytopchrome* promoters, inducing the transcription of *Period 1/2 and Cryptochrome 1/2,* with subsequent translation. As PER and CRY accumulate in the cytoplasm, the PER-CRY heterodimer forms and re-enters the nucleus, inhibiting CLOCK and BMAL1 and decreasing the transcription and translation of PER and CRY, thus lowering the concentration of PER and CRY in the cytoplasm. The inhibitory heterodimer degrades quickly, and *Per* and *Cry* translation resumes. Adapted from Takahashi et al., 2006, *Human Molecular Genetics*.

Glycogen Synthase Kinase 3, in the isoform GSK3β, is known to phosphorylate clock proteins PER2, CRY2, and REV-ERBα, clearly demonstrating its involvement in the cellular circadian rhythm (Hirota et al., 2008). Because lithium inhibits GSK3β, this suggests that at least some of lithium's effects may be enacted via alteration of patients' circadian rhythms

(Hirota et al., 2008; Porcu et al., 2019). Indeed, lithium is already known to lengthen circadian rhythms in humans (Johnsson et al., 1983), and has shown rhythm altering-effects in BD patients (McCarthy et al., 2019). Many clinical symptoms of BD, such as the prolonged wakefulness and nighttime activity in mania and the daytime sleeping and abnormal eating in depression, are considered clinical signs of circadian rhythm dysregulation. That the treatment for BD, lithium, is also implicated in the regulation of the molecular circadian clock indicates that circadian rhythms may be a key angle from which to approach the mechanisms and treatment of Bipolar Disorder.

1.4 Modelling Bipolar Disorder

The relationship between BD, lithium, and circadian rhythms remains undetermined in part because of the difficulty of modeling BD. In 2007, Roybal et al. used a dominant-negative *Clock* mutation, rendering CLOCK unable to activate *Per/Cry* transcription, to generate a mouse recreating many of the human symptoms of mania. The resultant mice were hyperactive, excessively involved in goal-directed and rewarding activities, and had reduced anxiety in open field tests. 0.4mM lithium treatment or viral-mediated CLOCK restoration in the ventral tegmental area, with the goal of correcting dopaminergic neuron hyperactivity, were each sufficient to return mouse activity and anxiety to wild-type levels (Roybal et al., 2007). Another mouse model of mood disorder was generated by Landgraf et al. in 2016 via stereotactic injection of viral vectors encoding short hairpin RNA (shRNA) targeting *Bmal1* in the suprachiasmatic nucleus. These *Bmal1* knock-down mice recreated human depressive symptomology, with greater helplessness, increased weight gain, and dysregulated production of the stress hormone corticosterone (Landgraf et al., 2016). Interestingly, the symptoms of both

mania and of depression can be modeled via disruption of core circadian regulators, such as *Clock* and *Bmal1*, connecting circadian rhythm dysregulation with BD mood states. However, a single mouse model that successfully recreates both mania and depression has not yet been created (Beyer and Freund, 2017). Therefore, to study an intact manic-depressive system, human models such as postmortem brains and fMRI have been used (Brennand et al., 2012; Viswanath et al., 2015). However, these models have both benefits and shortcomings: postmortem human brain slices can provide anatomical, cellular, and chemical information but cannot capture developmental or dynamic time-related aspects of BD, while fMRI yields longitudinal data but cannot provide information on molecular mechanisms (Brennand et al., 2012; Viswanath et al., 2015).

In vitro human fibroblasts, from skin samples donated by living BD patients, are useful because they reflect the genes present in BD patients and the full manic-depressive human BD phenotype and can provide a more direct route to the discovery of pharmacological interventions than would an animal model. As the fibroblasts are from already-characterized human patients, this model can be used in comparing an individual BD patient's clinical symptoms to their cells' molecular characteristics, potentially elucidating underlying molecular mechanisms of BD (McCarthy et al., 2013). These cultured human fibroblasts have allowed researchers to observe differences in the cellular circadian rhythms of BD patients and healthy controls (McCarthy et al., 2013), but BD is ultimately a disease of the brain. Converting these patient-derived fibroblasts into human induced pluripotent stem cells (iPSC) allows for more advanced cellular models. iPSCs can be differentiated into neuronal cells, allowing the molecular characteristics of living human brain cells to be studied. While fibroblasts, as peripheral cells, do not fire action potentials, form synaptic connections, or release neurotransmitters, the use of iPSC-derived

neurons corrects these shortcomings and allows for a model that more closely reflects the physiological factors occurring in a BD patients' brain. Furthermore, this model permits an unprecedented opportunity for cell-type-specific investigation and pharmacological testing, otherwise impossible in living BD patients. Human postmortem and magnetic resonance spectroscopy studies suggest that glutamate levels in the prefrontal cortex are dysregulated in BD and MDD patients relative to healthy controls; as such, we chose to differentiate the hiPSC into cortical glutamatergic neurons, a cell type which is known to be affected by the disease phenotype and may play a key role in the biological basis of BD (Jun et al., 2014).

Our current research extends the previous fibroblast circadian studies into neural progenitor cells (NPCs) and cortex-like glutamatergic neurons. Because these cells are derived from living BD patient donors whose clinical characteristics, such as lithium response vs. non-response, are already documented, we could sort neuronal lines by patient lithium response. To affirm that the molecular circadian rhythm differences between fibroblasts donated by BD patients vs. healthy controls were also present in neuronal cells, we performed rhythm analysis in cultured NPCs and neurons. Not only did we observe similar circadian rhythm abnormalities in BD neuronal cells as had been previously found in fibroblasts, we were also able to compare the circadian rhythms of immature cells (neural progenitor cells) and mature cells (neurons) in a way previously impossible using only mature fibroblasts.

We next evaluated NPCs and neurons for a differential response to *in vitro* lithium treatment. We hypothesized that lithium may have period-lengthening effects in the BD "lithium responder" and healthy control samples, as has been documented (Johnsson et al., 1983 in healthy human subjects; McCarthy et al., 2013, McCarthy et al., 2018 in BD fibroblasts). In circadian rhythm assays, we found that neural cells from known BD lithium responsive patients

(Li-R) displayed modest circadian differences from lithium non-responsive patient cells (Li-NR), and lithium treatment indeed affects control and BD Li-R cells dissimilarly from BD Li-NR cells. Ongoing analysis will reveal whether lithium's effect is complicated in immature vs. mature cell types. This may offer insight into the developmental component of BD, a disorder which is often diagnosed in young adulthood but likely begins much earlier, possibly prenatally (O'Shea et al., 2016). Using the iPSC-derived neuron model, we will also be able to evaluate other previously inaccessible properties of BD neurons, such as network formation and signalling activity, ultimately working towards characterizing these cells and gaining novel insight into the molecular mechanisms of BD.

Research using this hiPSC-derived neuron model may contribute to the eventual creation of a cell-based pharmacological screening method, in which patient skin samples could be used to determine whether patients are likely lithium responders or non-responders before they are prescribed the drug. Compared to the current trial-and-error process, this has the potential to be more time and cost-efficient for healthcare professionals and patients, and ultimately could help more BD patients reach clinical maintenance.

MATERIALS AND METHODS

2.1 Human Subjects

Patients diagnosed with bipolar disorder type I were recruited from the Pharmacogenetics of Bipolar Disorder (PGBD) trial, a prospective lithium monotherapy clinical study designed to identify clinically responsive BD patients (Oedegard et al., 2016). Controls were recruited separately from another study (Mertens et al, 2015). Written informed consent was obtained from all subjects. Bipolar disorder subjects were transitioned to lithium monotherapy gradually and clinically assessed every 2-8 weeks for 24 months. Clinical stability was measured using the Clinical Global Impressions (CGI) Scale. Patients with CGI scores indicating "absent-mild symptoms" who maintained clinical stability were considered Li responders. Subjects who had unstable mood symptoms or suffered from a relapse were considered non-responders (Oedegaard et al, 2016). Table 1.1 describes the clinical characteristics of BD and control subjects.

Table 2.1: Clinical characteristics of control and BD subjects. Four control subjects and six BD patients were recruited. All subjects selected as cell line donors were adult Caucasian males and all BD subjects had been previously received a diagnosis of BD type 1. BD subjects were divided into Lithium (Li) Responder and Non-Responder groups based on their response to Lithium monotherapy as described above. Asterisks indicate two subjects whose cell lines were not differentiated into NPCs and so were not included in the experiments described in this thesis.

Subject	Group	Age	Diagnosis
1	Control	56	None
2	Control	73	None
3	Control	38	None
4	*Control	33	None
5	Li Responder	57	BD I, PTSD, ADHD
6	Li Responder	65	BD I
7	*Li Responder	59	BD I, PTSD
8	Li Non-Responder	54	BD I, PTSD
9	Li Non-responder	22	BD I, ADHD
10	Li Non-responder	69	BD I

2.2 hiPSC Culture

BD and control subject fibroblast samples were converted into human iPSC (hiPSC) using the Cyto-Tune Sendai reprogramming kit (ThermoFisherSci) in the Fred Gage Lab (Mertens et al, 2015). Cryopreserved hiPSC samples were thawed in the McCarthy lab and cultured in 6 well plates in a Nuaire Water-Jacketed IR Autoflow CO2 incubator with 5% CO2 at 35°C. The substrate used was matrigel (BD Biosciences) and the growth media was mTeSR+ (Stem Cell Tech #85850, consisting of hiPSC basal media, mTeSR supplement, and Penicillin/Streptomycin 1:100 (Bio Core)), replaced daily. Rough-edged colonies and cells

lacking multiple visible nuclei were considered indicative of non-iPSC identity, and these cells were removed manually using L- shaped glass micropipette "hooks" manipulated under brightfield microscopy. For transfer, cells were washed in DMEM F12 and dissociated using collagenase IV (Stem Cell Tech #7909), then colonies were lifted from the plate using cell lifters (Corning) and centrifuged at 900 rpm for 2 minutes. Cells were then re-suspended in one of several types of media depending on the operation required. For propagation, conducted once weekly or as necessary based on density, cells were resuspended in mTeSR+ media and plated in matrigel-coated 6 well plates at a 1:3 expansion ratio. For preservation, cells were resuspended in a preservation media consisting of 70% Knock-out Serum Replacement (Fisher Scientific #10828010), 20% mTeSR+ Media, and 10% DMSO (Sigma) and the solution was immediately aliquoted into cryotubes and placed at - 80C. For further differentiation into Embryoid Bodies, cells were resuspended in MTeSR+ media and plated in 6-well ultra-low attachment plates (Corning).

2.3 Embryoid Body Cell Culture

Embryoid Bodies (EBs) were grown in 6-well ultra-low attachment plates without substrate and were fully suspended in neural induction medium (NIM: DMEM F12/Glutamax supplemented with N2/B27 (Invitrogen) and Penicillin/Streptomycin 1:100), which was replaced every other day. After one week in culture, EBs were plated on poly-L-ornithine/laminin (Sigma #P3655) coated plates. NIM media changes continued every other day as the colonies adhered to the plate surface and began to form neural rosettes.

2.4 Neural Rosette Cell Culture

Neural Rosettes were grown in 6-well plates on poly-L-ornithine/laminin substrate using NIM, which was replaced every other day. After one week in culture, developed rosettes were manually removed from the well using a scalpel under brightfield microscopy. Excised rosettes were dissociated using accutase (Stem Cell Tech #7920) and re-plated as single cells on poly-L-ornithine/laminin-coated plates for differentiation into neural progenitor cells (NPCs).

2.5 Neural Progenitor Cell Culture

NPCs were grown on poly-L-ornithine/laminin substrate using neural proliferation medium (NPM: NIM supplemented with 20ng/mL fibroblast growth factor 2 (Peprotech)), which was replaced every other day. NPCs were maintained at high confluency to prevent differentiation. After one week in culture, NPCs were washed in Dubecco's Phosphate-Buffered Solution (DPBS) and dissociated using accutase, then centrifuged at 1800 rpm for 2 minutes. Cells were then re-suspended in one of several types of media depending on the operation required. For propagation, conducted once weekly or as necessary based on confluence, cells were resuspended in NPM and plated in polyornithine/laminin-coated 6-well plates at a 1:3 expansion ratio. For cryopreservation, cells were resuspended in preservation media consisting of 90% NPM and 10% DMSO and the solution was immediately aliquoted into cryotubes and placed at -80°C. For further differentiation into neurons, cells were resuspended in NPM. A sample of the solution was extracted and mixed with trypan blue so that cell density could be measured using a hemocytometer under brightfield microscopy. Cells were plated on matrigel-coated 35mm dishes at either $200x10^3$ cells/well or $90x10^3$ cells/well.

2.6 Neuron Cell Culture

Neurons were grown in 35mm dishes on matrigel substrate using neural differentiation medium (NDM: NIM supplemented with 20ng/ml brain derived neurotrophic factor (Peprotech), 20ng/ml glial cell line-derived neurotrophic factor (Peprotech), 1mm dibutyryl-cyclic adenosine monophosphate (Sigma), 200nM ascorbic acid (Sigma)), with half media changes once per week. Neurons developed extensive morphological arborization and neural circuitry over a four to eight week maturation period. By four weeks of maturation, cells were found via immunocytochemistry to express neuron-specific markers such as β-III tubulin.

2.7 Immunocytochemistry

To confirm that cells displayed the stage-specific markers associated with each subsequent stage of differentiation, immunocytochemistry was conducted on iPSC, NPCs, and neurons. iPSC were cultured on matrigel-coated glass coverslips and NPCs and neurons were cultured on poly-L-ornithine/laminin-coated glass coverslips. When the desired density of cells was achieved, media was removed and cells were washed in DPBS and fixed using 4% paraformaldehyde. After 30 minutes in paraformaldehyde, cells were washed twice in DPBS and permeabilized using 0.2% TritonX-100 (Sigma #X100) diluted in DPBS. Coverslips were placed in a wet chamber and incubated in 5% donkey serum (Jackson ImmunoResearch #017-000-121) for one hour to block non-specific proteins. Next, the primary antibodies (Table 2) under consideration, diluted in 2% donkey serum, were added to the coverslips. Coverslips were incubated at 4°C overnight. The following day, coverslips were washed three times using 0.2% TritonX-100 diluted in DPBS and then incubated in secondary antibodies (1:500) diluted in 2% donkey serum for two hours at 21°C. Coverslips were washed in DPBS and incubated in DAPI

(ThermoFisher Sci #D1306) for five minutes, then washed in dH2O and mounted on slides using aqueous mounting medium (Polysciences, Inc #18606-20). Visualization was conducted via bioluminescence microscopy (Leica Microsystems #C2343-33722164).

Table 2.2: Antibodies used for immunocyotchemistry.

Target	**Species**	**Company**	**Cat #**	**Dilution**
TUJ-1	Mouse	Biolegend	801201	1:300
GFAP	Goat	Abcam	ab53554	1:600
NESTIN	Mouse	Millipore	MAB5326	1:200
SOX2	Rabbit	Cell Signalling Tech	3579S	1:200
TRA -1-60	Mouse	Millipore	MAB4360	1:300
NANOG	Goat	R&D Systems	AF1997-SP	1:400
VGLUT2	Mouse	Synaptic Systems	135 421	1:300
PER2	Rabbit	Abcam	ab179813	1:300
PER1	Rabbit	Abcam	ab136451	1:300

2.8 Gene Expression Analysis using Quantitative Rolymerase Chain Reaction (qPCR)

RNA was isolated from NPCs and neurons plated at 400 x 10^3 cells/well. NPCs were dissociated using accutase and plated on 6 well plates, then allowed to re-adhere for 48 hours. Neurons were plated on matrigel-coated 35mm dishes and were allowed to mature for 4-8 weeks as described above. When maturation and cell adherence was sufficient, as determined via brightfield microscopy, cell media was removed and replaced with forskolin (10uM, Tocris), a circadian-rhythm synchronizing agent which interacts with downstream signalling transduction pathways which may in turn stimulate the circadian clock system. After three hours of forskolin

stimulation, cells were washed in DPBS and placed in fresh stage-appropriate media, then incubated at 35°C for 12 hours. After 12 hours, cells were collected at 6 hour intervals, with two replicate wells from each cell line frozen at each time point. Wells were washed with 4°C DPBS (Thermo Scientific), all media was completely aspirated, and the plates were wrapped in plastic wrap and snap-frozen at -80°C until RNA extraction.

RNA was extracted using the Qiagen RNeasy kit (Qiagen #74104) as per manufacturer's instructions. Frozen cells from control and patient cell lines were processed on one date. Cells were lysed using lysis buffer and β-Mercaptoethanol. The contents of the wells were removed using a cell lifter and pooled into Eppendorf tubes and frozen. Four tubes were prepared for each cell line, corresponding to one sample per time point. After centrifugation, the supernatant was removed via aspiration and an equal volume of 70% ethanol was added to the supernatant before the contents of the tube were transferred to an RNeasy Mini spin column and centrifuged. Columns were next washed once with Buffer RW1, then twice with Buffer RPE. The flowthrough was discarded following each centrifugation. RNA was eluted from the columns using 50uL RNase-free water and columns were washed again with the flowthrough to ensure sufficient elution. The NanoDrop 2000 (ThermoFisher Sci) was used to quantify total RNA. For each sample, 500ng of total cellular RNA was removed and used to generated cDNA via the High Capacity cDNA Reverse Transcription Kit (Applied Biosystems #4368814) and T100 Thermal Cycler (Bio-Rad #1861096). Taqman qRT-PCR was conducted using the C1000 Touch Thermal Cycler and CFX384 Real-Time System (Bio-Rad), with Taqman probes selected to measure key individual components of the positive and negative limbs of the circadian clock (*PER1/2, CRY1/2, BMAL1, CLOCK*). *GAPDH* was used as a housekeeping control gene to calculate fold change difference in gene expression across the four timepoints.

2.9 Circadian Rhythm Recording: Recording via Luminometer

Circadian rhythms were recorded from NPCs and neurons plated at 250 x 10^3 cells per well. NPCs were dissociated using accutase and plated on matrigel-coated 35mm dishes, then allowed to re-adhere for 48 hours. Neurons were initially plated on matrigel-coated 35mm dishes and were allowed to mature for 6 – 10 weeks as described above. NPCs and neurons were transduced using the surfactant polybrene and a lentiviral *Per2-luc* construct, diluted in neural proliferation media (NPCs) or neural differentiation media (neurons), respectively. After 48 h of incubation, media was removed and replaced with stage-appropriate media containing 10uM forskolin (Tocris) to synchronize rhythms. After two hours of forskolin incubation, cells were washed in DPBS and placed in recording media (DMEM (Invitrogen 12100046, serum-free, 1.2g/L sodium bicarbonate, pH 7.41) 10mM HEPES, a bicarbonate buffer solution, 25 U/mL penicillin, 25 ug/mL streptomycin, 2%B-27 (GIBCO 17504-044), 1mM luciferin). 35mm dishes were made airtight using a grease seal and placed inside a 32-channel LumiCycle luminometer (Actimetrics) housed inside a dry incubator set to 35°C without CO2. Bioluminescence recording occurred for 70 seconds every 10 minutes for five to seven days. Temperature was maintained at 35°C for the duration of recording. Patient and control cell lines were recorded in triplicate.

For recordings during temperature cycles, the temperature within the LumiCycle luminometer alternated between 35°C and 37.5°C in a pre-programmed 12 hour: 12 hour cycle. All other cell preparation and recording parameters were as described above.

For recordings involving pharmacological manipulation, 1mM and 10mM Lithium Chloride was added to the recording media immediately before luminometry began. Temperature was maintained at 35°C for the duration of recording. BD and control cell lines were recorded in at least duplicate for each experimental condition, e.g. two vehicle, two 1mM, and two 10mM

35mm dishes were prepared for each cell line during each trial. All other cell preparation and recording parameters were as described above.

2.10 Single-Cell Recording via Time-Lapse Bioluminescence Microscopy

The circadian rhythms of individual cells were recorded using NPCs and neurons plated at $90x10^3$ cells per well. NPCs were dissociated using accutase and plated on matrigel-coated 35mm dishes, then allowed to re-adhere for 48 hours. Neurons were initially plated on matrigel-coated 35mm dishes and were allowed to mature for 6 – 10 weeks as described above. NPCs and neurons were transduced using the surfactant polybrene and a lentiviral *Per2-luc* construct, then synchronized with forskolin as described above. 35mm dishes were made airtight and placed on the stage of a bioluminescence microscope (Olympus, Tokyo, Japan, using an Olympus 4x XLFLUOR objective (NA 0.28)) transmitting to a cooled charge-coupled-device camera (Series 800, Spectral Instruments, Tucson, AZ, USA). Bioluminescence was recorded every 30 minutes with an exposure time of 29.5 minutes for each image. Temperature was maintained at 36°C for the duration of recording. Recording continued for five to seven days and images were compiled into a time-lapse video for analysis, which was conducted using MetaMorph (Universal Imaging Corp., Buckinghamshire, UK).

2.11 Data Analysis

Single-cell bioluminescence microscopy images were compiled into a time-lapse video using the MetaMorph software. Fields containing one cell were defined manually and objective brightness over time was logged into Microsoft Office Excel via MetaMorph, generating a text-

coverted sine wave file for each cell. Further analysis of each cell's circadian rhythm was conducted using the LumiCycle program.

Analysis of circadian rhythms at both population and single cell level was conducted using LumiCycle software (Actimetrics, Inc.). The first 0.8 days of data generally contained artefacts related to sample transport or media change and were excluded. In the LumiCycle analysis software, rhythms were fit to a damped sine curve to calculate period and phase measurements, and an un-damped sine curve to calculate amplitude. Recordings that deviated significantly from the best fit curve, i.e. had a low "goodness of fit", and were determined to be arrhythmic via spectral power analysis were excluded from period and phase analysis. Rhythms that had a period less than 18 or greater than 28 were considered outliers and excluded from period analysis. Values were imported to Microsoft Office Excel. Statistical analysis was performed using GraphPad Prism version 5: One-way analysis of variance (ANOVA) and t-test were used to assess differences in amplitude and period between diagnosis groups. Two-way ANOVA was used to analyze differential response to lithium treatment among diagnosis groups or changes over time in gene expression. For single cell rhythms, phase values were converted to polar coordinates and screened for rhythmicity (period 18-28 hours, Fast Fourier Transform (FFT) peak > 0.15). Individual cell phase values were plotted on a polar graph using Oriana software and analyzed for clustering using Rayleigh's test and measurement of the mean vector. In all tests a p-value < 0.05 was used to determine statistical significance.

RESULTS

3.1 Culture of hiPSC-Derived Neurons

Fibroblasts from BD patients and healthy controls have previously been reprogrammed into hiPSC and differentiated into glutamatergic neurons by Mertens et al. (2015). To ensure that hiPSC differentiation progressed successfully, we visually examined cell morphology via brightfield microscopy at each stage of differentiation **(Figure 3.1A-E)** and performed immunocytochemistry on cells in the hiPSC, NPC, and neuron stages to verify cellular identity. hiPSC expressed pluripotency markers NANOG and TRA-1-60 **(Figure 3.1F)**, NPCs expressed neuro-ectodermal marker NESTIN and progenitor marker SOX2 **(Figure 3.1G)**, and neurons expressed neuron-specific β-III tubulin **(Figure 3.1H)**, confirming cell identity at each respective stage. Astrocytes were produced along with the neurons, as shown by the minority of cells expressing glial fibrillary acidic protein (GFAP) **(Figure 3.1H)**. β-III tubulin colocalized with markers for vesicular glutamate transporter 2 (VGLUT2), indicating the successful culture of glutamatergic neurons **(Figure 3.1I)**. These findings confirm that fibroblast-derived hiPSC were differentiated along the neuronal development pathway into NPCs and glutamatergic neurons, making them suitable for further circadian rhythm analysis.

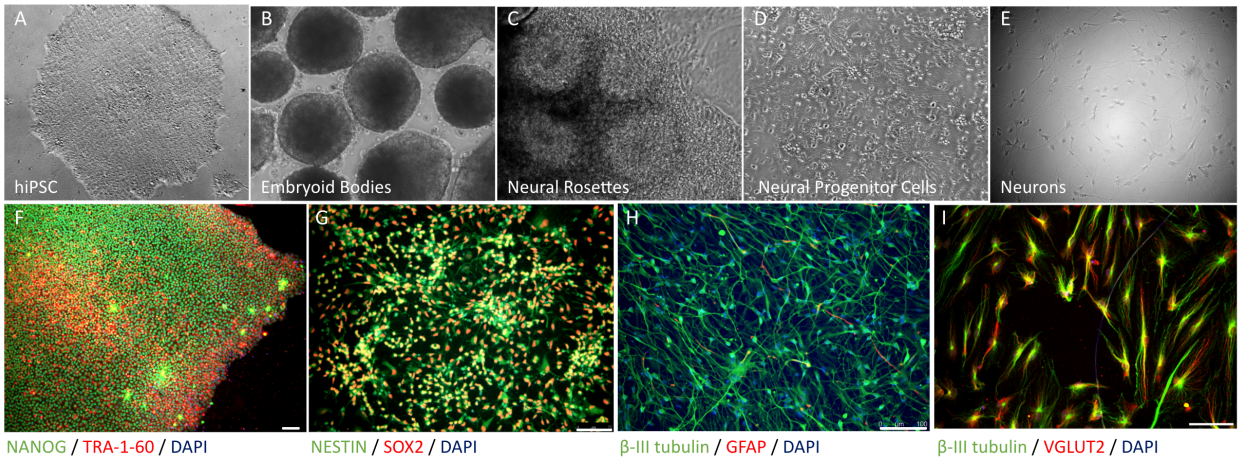

Figure 3.1: Patient and control fibroblast-derived hiPSC are differentiated into glutamatergic neurons. Fibroblasts from healthy control and BD patient human donors were reprogrammed into hiPSC and underwent differentiation into cortex-like glutamatergic neurons. **(A-E)** hiPSC and hiPSC-derived cells were visualized via brightfield microscopy at 10X magnification. **(A)** An hiPSC colony with clearly delineated borders, a roughly circular shape, and a singular layer of round cells. **(B)** Multiple Embryoid Bodies (EBs) suspended in media. EBs appear roughly spherical in shape and are opaque under brightfield microscopy. **(C)** Four neural rosettes with "donut-like" morphology, each representing a primitive neural tube. A scalpel was used to cut around the outer border of the rosette to isolate neuroepithelium-like cells for further differentiation into the NPC stage. **(D)** Neural progenitor cells (NPCs) in a single cell layer, maintained in a semi-confluent state. Some neurites are visible. **(E)** Neurons with defined cell bodies and multiple long neural projections. **(F-I)** Immunocytochemistry of hiPSC-derived cells. All cells were stained with nuclear marker DAPI (blue) and visualized via fluorescence microscopy. **(F)** hiPSC expressing pluripotency markers NANOG (green) and TRA-1-60 (red). Scale bar =50um. **(G)** NPCs expressing neuro-ectodermal marker NESTIN (green) and progenitor marker SOX2 (red). Scale bar = 75um. **(H)** Neurons expressing neuron-specific β-III tubulin (green) and astrocytes expressing GFAP (red). Scale bar = 100um. **(I)** Neurons expressing co-localized β-III tubulin (green) and vesicular-glutamate transporter 2 (VGLUT2). Scale bar = 100um.

3.2 Expression of Core Circadian Clock Genes is Increased in Bipolar Disorder NPCs and Neurons

Bipolar Disorder patients have been found to have altered circadian rhythms, even during periods of euthymia, suggesting that BD-associated circadian dysregulation may be biologically inherent and present at the cellular level (McCarthy et al., 2019). To determine if the gene expression levels of key components of the molecular circadian clock differ BD cells vs. healthy controls, and how these expression levels fluctuate over a day, my colleagues Angelica Luis and Himanshu Mishra performed 24 hour time-course Quantitative Reverse Transcription PCR (qRT-PCR) analysis. *PER2, CRY1, BMAL1,* and *CLOCK* expression were examined in NPCs **(Figure 3.2A-D**) and neurons **(Figure 3.2E-H)** to capture any effects of cell development.

The expression levels of *PER2* and *CRY1*, negative transcriptional regulators within the Transcriptional-Translational Feedback Loop (TTFL) were significantly elevated in BD NPCs and neurons **(Figure 3.2C, D, G, H)**. For *BMAL1* and *CLOCK*, positive transcriptional regulators in the TTFL, expression was not significantly different from controls in the NPC stage **(Figure 3.2A, B)**. However, in BD neurons *BMAL1* expression was elevated compared to controls, **(Figure 3.2E)**, though *CLOCK* expression was not significantly different between BD and control neurons **(Figure 3.2F)**. This suggests that BD neurons express a dysregulated molecular circadian clock, and this dysregulation is present at the NPC stage of development. In both NPCs and neurons, no differences in gene expression across time were detected, indicating that this assay does not convey information about how gene expression rises and falls throughout a circadian day.

Figure 3.2: Expression of PER2 and CRY1 is increased in BD NPCs and neurons. Quantitative Reverse Transcription PCR (qRT-PCR) was performed on NPC and neuron samples collected at t = 6, 12, 18, and 24 h over a 24 hour time-course experiment. Probes for core circadian clock genes *BMAL1, CLOCK, CRY1,* and *PER2* were used, and line graphs show respective gene expression levels at each time point. Error bars indicate standard error of mean (SEM). Control cell gene expression is shown in black and pooled BD Li Responder and BD Li Non-Responder gene expression is shown in red. Data was analyzed with two-way ANOVA: * indicates a main effect of diagnosis ($p < 0.05$). There were no significant effects of time or time x diagnosis interactions. For each probe, expression levels were normalized to the mean level of gene expression in control NPCs or neurons (dotted line). In NPCs **(A-D)**, Controls: n = 3-5 replicate cell lines derived from 2 healthy donors, BD: n = 7-10 replicates from 3 patient donors. In neurons **(E-H)**, Controls: n = 4-5 replicates from 2 donors, BD: n = 7-10 replicates from 5 donors. Data collected by Angelica Luis and Himanshu Mishra.

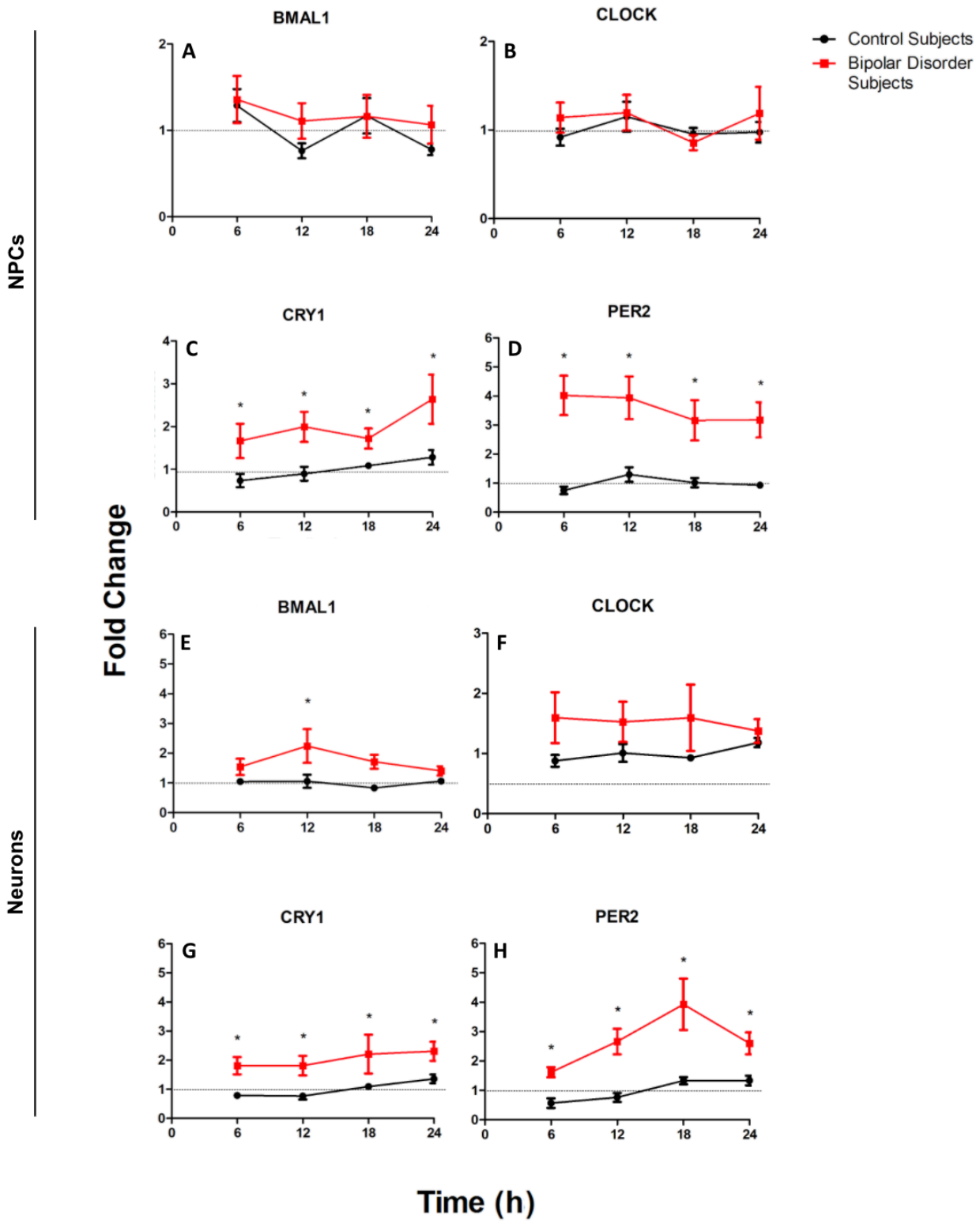
NPCs
Neurons
BMAL1
CLOCK
CRY1
PER2
A
B
C
D
E
F
G
H
Control Subjects
Bipolar Disorder Subjects
Fold Change
Time (h)

Figure 3.2

3.3 Circadian Rhythm Parameters Differ Between Control, BD Li Responder, and BD Li Non-Responder Cells

In order to examine circadian rhythms in the expression of key components of the molecular circadian clock in more detail, we used *Per2-luc*, a bioluminescent reporter-based assay that permitted multiple consecutive days of rhythm recording, based on earlier work in fibroblasts (McCarthy et al., 2013). We chose to focus on *Per2-luc* expression, as *Per2* is a known core regulator of the molecular circadian clock, couples to other genes in the TTFL, and can therefore be considered representative of the overall activity of the clock. Our prior RT-qPCR experiments also suggest that *Per2* expression is differentially regulated in BD NPCs and neurons as compared to healthy control cells **(Figure 3.2)**, indicating that regulation of *Per2* may contribute to the molecular mechanism of BD circadian disruption.

We first tested our *Per2-luc* reporter-based circadian rhythm assay to ensure that hiPSC-derived NPCs and neurons demonstrated rhythmic *Per2-luc* activity during cell population-level recordings. NPCs **(Figure 3.3A, B, C)** and neurons **(Figure 3.3G, H, I)** exhibited robust bioluminescence rhythms, hereafter assumed to reflect molecular circadian rhythms, with an observed trend towards greater rhythm amplitude in healthy control-derived cell populations, lesser amplitude in BD Li Responder cell populations, and low amplitude in BD Li Non-Responder cell populations.

We next analyzed the rhythm parameters of each diagnosis group separately. In both NPCs **(Figure 3.3D)** and neurons **(Figure 3.3J)** average circadian rhythm amplitude was significantly higher in control cells and BD Li-R cells as compared to BD Li-NR cells. There was no significant difference between control and BD Li-R cell average amplitude, indicating that across developmental stages, BD Li-NR patient cells may have less robust *Per2* expression,

and potentially less robust molecular circadian rhythms, than do BD Li-R and healthy subject cells.

In NPCs, average circadian rhythm period was significantly shorter in cells derived from either BD patient group compared to cells from healthy controls (average period: Control = 24.99 ± 0.60 hr, BD = 23.06 ± 0.29 hr, $p < 0.003$; **Figure 3.3E, F)**. In neurons, the trend of longer rhythm period in control cells and shorter period in BD patient cells continued, although the difference in circadian period was not significant (average period: Control = 24.63 ± 0.28 hr, BD = 24.15 ± 0.37 hr; **Figure 3.3K, L)**. Furthermore, the McCarthy lab has previously found an association between circadian period and lithium response in BD-patient derived fibroblasts (McCarthy et al., 2013; McCarthy et al, 2019).

Figure 3.3: Circadian rhythm amplitude and period differ between Control, BD Li Responder, and BD Li Non-Responder cells. Cells were transduced with a *Per2-luc* lentiviral reporter and a luminometer was used to record bioluminescence over a 5-day period. The signal recorded from each sample was used to produce a best-fit sine wave to estimate rhythm parameters. **(A-C)** Representative traces from NPC **(A)** Control, **(B)** BD Li-R, and **(C)** BD Li-NR cell populations. The colored lines indicate the bioluminescence emitted by a single 35mM dish of cells plated at 250 x 10^3 cells/well, and the black line indicates the best-fit damped sine curve generated by the LumiCycle Analysis software. **(D)** Average circadian rhythm amplitude in NPCs. For each cell line, the average rhythm amplitude across all trials was calculated, and averages were pooled by diagnostic group (Control = 0.0612 ± 0.006 counts/sec, BD Li-R = 0.0632 ± 0.011 counts/sec, BD Li-NR = 0.0349 ± 0.003 counts/sec). One-way ANOVA revealed a significant difference between Control and BD Li-NR and between BD Li-R and BD Li-NR ($p < 0.004$). There was no significant difference between Control and BD Li-R average rhythm amplitudes. **(E)** Average circadian rhythm period in NPCs. For each cell line, the average rhythm period across all trials was calculated, and averages were pooled by diagnostic group (Control = 24.99 ± 0.579 hr, BD Li-R = 22.96 ± 0.758 hr, BD Li-NR = 23.11 ± 0.215 hr). One-way ANOVA revealed a significant difference between Control and both BD Li-R and BD Li-NR ($p < 0.004$). There was no significant difference between BD Li-R and BD Li-NR rhythm period. **(F)** Average circadian rhythm period in NPCs, with combined BD Li-R and BD Li-NR data (Control = 24.99 ± 0.579 hr, BD = 23.06 ± 0.288 hr). Two-tailed, unpaired T Test revealed a significant difference between Control and BD period ($p < 0.003$). **(G-I)** Representative traces from neuron **(G)** Control, **(H)** BD Li-R, and **(I)** BD Li-NR cell populations. **(J)** Average circadian rhythm amplitude in neurons (Control = 0.0667 ± 0.009 counts/sec, BD Li-R = 0.0735 ± 0.011 counts/sec, BD Li-NR = 0.0373 ± 0.005 counts/sec). One-way ANOVA revealed a significant difference between Control and BD Li-NR and between BD Li-R and BD Li-NR ($p < 0.004$). There was no significant difference between Control and BD Li-R amplitudes. **(K)** Average circadian rhythm period in neurons (Control = 24.63 ± 0.276 hr, BD Li-R = 24.31 ± 0.754 hr, BD Li-NR = 24.06 ± 0.386 hr). No significant difference was found between diagnosis groups. **(L)** Average circadian rhythm period in neurons, with combined BD Li-R and BD Li-NR data (Control = 24.63 ± 0.276 hr, BD = 24.15 ± 0.368 hr). No significant difference was found between diagnosis groups. In NPCs, n=3 control subjects, 2 BD Li-R, and 2 BD Li-NR cell lines, each recorded in triplicate during each of three separate experimental trials. In neurons, n=3 control subjects, 2 BD Li-R, and 3 BD Li-NR cell lines, each recorded in triplicate during each of five separate experimental trials.

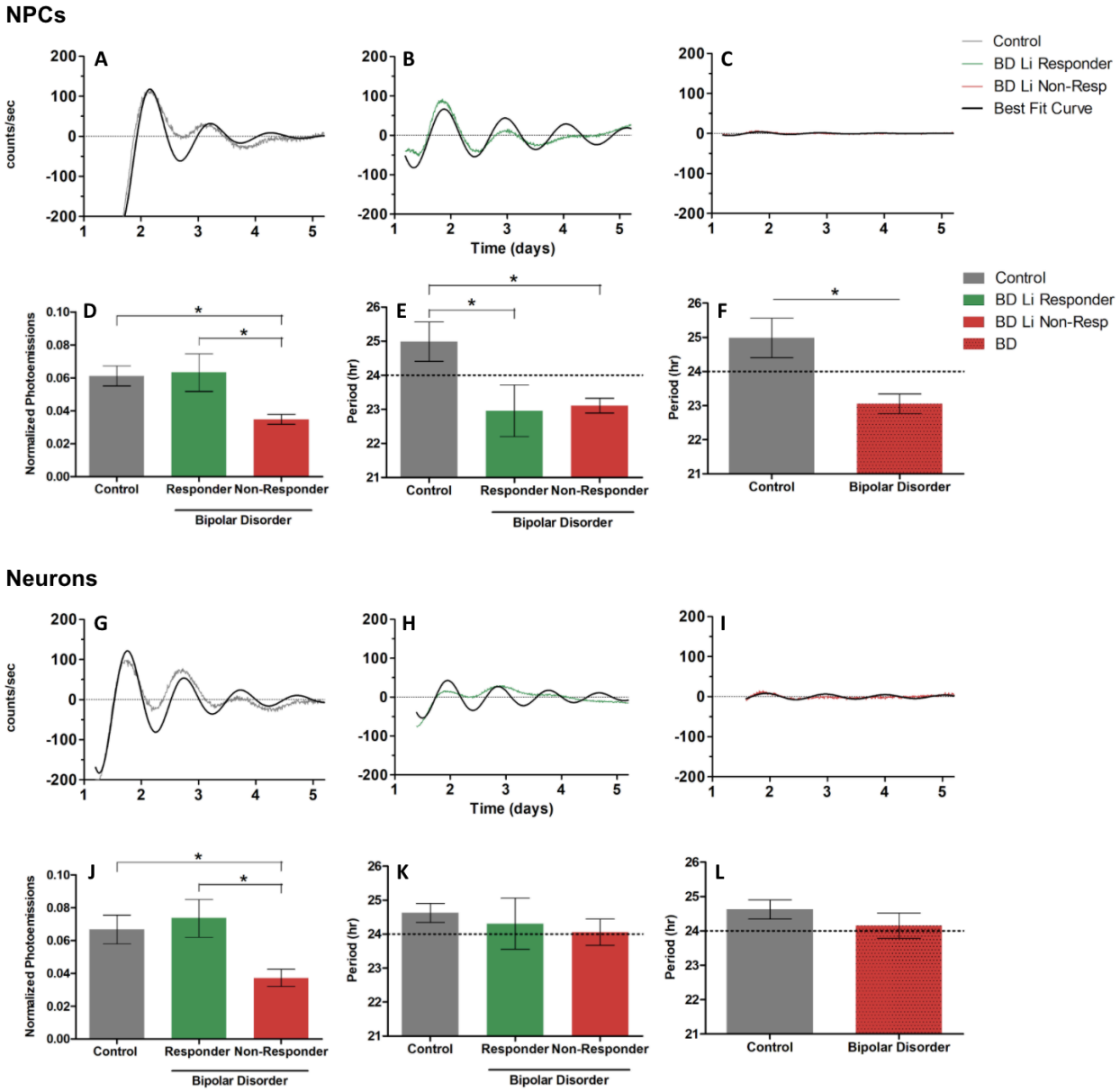
NPCs
A
B
C
Control
BD Li Responder
BD Li Non-Resp
Best Fit Curve
counts/sec
Time (days)
D
E
F
Normalized Photoemissions
Period (hr)
Control
Responder
Non-Responder
Bipolar Disorder
BD
Neurons
G
H
I
J
K
L

Figure 3.3

3.4 Effects of Lithium on Period

Lithium, a mood stabilizing medication used to treat BD, is known to lengthen circadian rhythm period in healthy humans (Johnsson et al., 1983) and has been shown to affect molecular circadian rhythms in BD patient-derived fibroblasts (McCarthy et al., 2019). Extending this work previously done in peripheral cells, we treated NPCs and neurons with 1mM and 10mM lithium before performing circadian rhythm recording and analysis.

In NPCs, compared to control subjects, lithium reduces the amplitude of circadian rhythms in BD Li Responder cells **(Figure 3.4A)**. This effect was concentration-dependent, with rhythm amplitude decreasing successively with 1mM and 10mM lithium treatment. No significant effect of lithium treatment was found in BD Li Non-Responders. Two-way ANOVA revealed a significant effect of diagnosis ($p < 0.008$), lithium ($p < 0.003$) and diagnosis x lithium interaction ($p < 0.03$) on circadian rhythm amplitude. This indicates that in NPCs, control and BD patient cell amplitude responds to lithium treatment and that this cellular response is distinct among samples from controls, BD Li-R, and BD Li-NR. In neurons, two-way ANOVA revealed a significant effect of diagnosis ($p < 0.003$) **(Figure 3.4D)**, indicating that control, BD Li-R, and BD Li-NR average circadian rhythm amplitudes were different, but rhythm amplitude was not affected by lithium treatment. In agreement with **Figure 3.3D, J**, in both NPCs and neurons there was a trend of reduced rhythm amplitude in BD Li-NR cells, regardless of Li concentration, vs. control subject and BD Li-R cells.

In NPCs, when circadian period was normalized to the average circadian period of vehicle-treated control cells two-way ANOVA revealed a significant effect of diagnosis ($p < 0.0003$) and diagnosis x lithium interaction ($p < 0.02$) **(Figure 3.4C)**. In neurons, two-way ANOVA revealed a significant effect of diagnosis ($p < 0.02$) and lithium ($p < 0.006$) on

circadian period **(Figure 3.4E)**. In control and BD Li-R cells there was a trend of concentration-dependent circadian period lengthening, while in BD Li-NR cells this effect was absent **(Figure 3.4F)**. This indicates circadian period can be modulated via lithium treatment in the NPC stage, although response in NPCs shows no clear trend. In mature neurons, control and BD Li-R cells may respond to lithium treatment in a similar way, i.e. circadian period lengthening, while BD Li-NR cells appear to have little/no response to lithium treatment, possibly as a result of a dysregulation of the molecular circadian clock unique to this diagnosis group. Further repetition of these currently limited lithium trials, particularly in NPCs, may clarify the effects of lithium treatment on circadian amplitude and period.

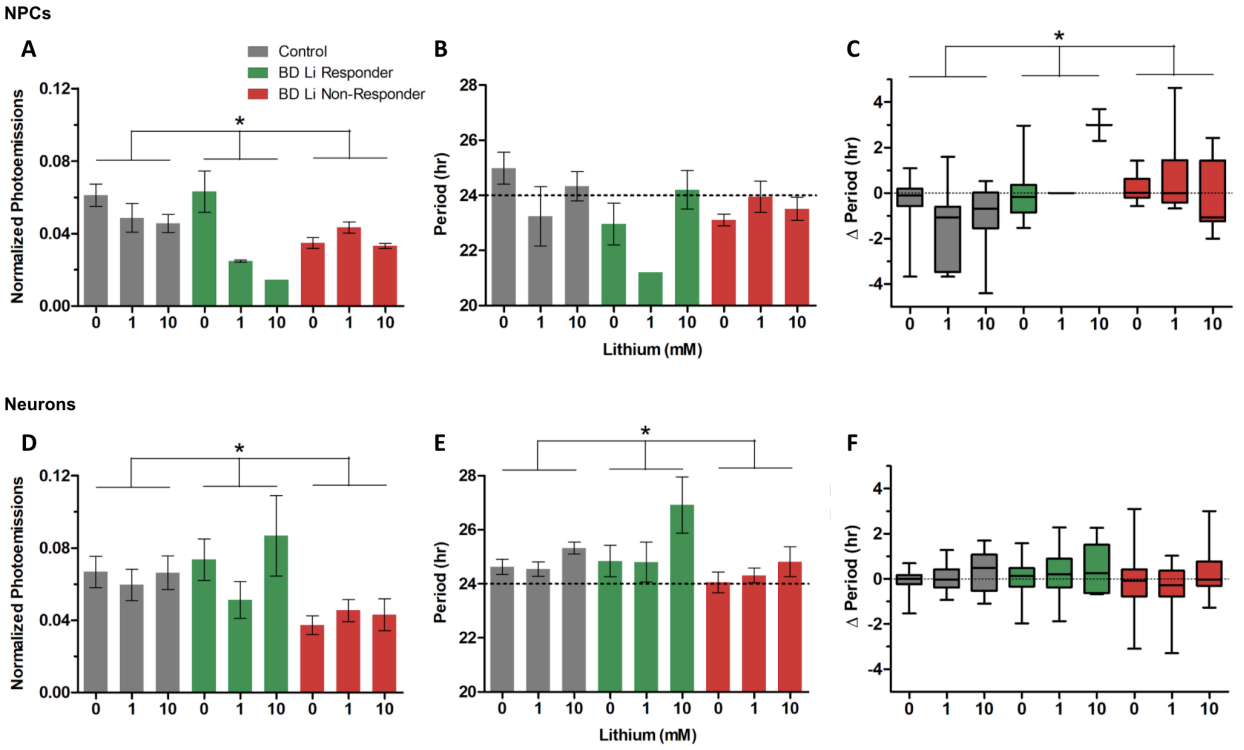

Figure 3.4: Lithium mediates concentration-dependent circadian period lengthening in Control and BD Li Responder neurons. Neurons were transduced with a *Per2-luc* lentiviral reporter and 1mM or 10mM Lithium Chloride (Li) was added to cell media immediately prior to recording. A luminometer was used to record bioluminescence over a 5-day period. **(A)** Average circadian rhythm amplitude in NPCs. For each cell line, the average rhythm amplitude across all trials was calculated, and averages were pooled by diagnostic group and Li concentration. Two-way ANOVA revealed a significant effect of diagnosis ($p < 0.008$), Li ($p < 0.003$), and diagnosis x Li interaction ($p < 0.03$). **(B)** Average circadian rhythm period in NPCs. For each cell line, the average rhythm period across all trials was calculated, and averages were pooled by diagnostic group and Li concentration. No significant difference was found between diagnosis groups. **(C)** Average change in circadian rhythm period in NPCs. For each cell line, the average rhythm period across all trials was calculated and averages were pooled by diagnostic group and Li concentration, then expressed as a fold difference over the average rhythm period of vehicle-treated Controls. Two-way ANOVA revealed a significant effect of diagnosis ($p < 0.0003$) and diagnosis x Li interaction ($p < 0.02$). **(D)** Average circadian rhythm amplitude in neurons. Two-way ANOVA revealed a significant effect of diagnosis ($p < 0.003$). **(E)** Average circadian rhythm period in neurons. Two-way ANOVA revealed a significant effect of diagnosis ($p < 0.02$) and Li ($p < 0.006$). **(F)** Average change in circadian rhythm period in neurons. No significant difference was found between diagnosis groups. In NPCs, n=3 control subjects, 2 BD Li-R, and 2 BD Li-NR cell lines, each recorded in duplicate or triplicate for each experimental condition (vehicle, Li 1mM, Li 10mM) during each of three separate experimental trials. In neurons, n=3 control subjects, 2 BD Li-R, and 3 BD Li-NR cell lines, each recorded in duplicate or triplicate for each condition during each of five separate experimental trials.

3.5 Single Cell Analysis Reveals Lower Rhythmicity and Disparate Rhythm Phases in BD NPCs Compared to Control Cells

Single cell analysis permits the examination of the molecular circadian rhythm occurring in an individual cell. Population-level recording, while yielding high-amplitude circadian rhythms **(Figure 3.3A-C, G-I)** assumes that cells within a sample are in relative synchrony. Cells oscillating out of phase with the population could produce a high level of "background" light emission and generate destructive interference, resulting in population-level rhythms that appear low-amplitude or dampen rapidly as cells fall out of synchrony (Welsh et al., 2004). Previous analysis of *Per2-luc* transduced, dissociated rodent fibroblasts and SCN neurons has found that dispersed cells are capable of maintaining completely autonomous circadian rhythms, but within a sample these rhythms have randomly-distributed phases (Welsh et al, 2004; Welsh et al., 2010).

We screened individual cells' bioluminescence outputs for rhythmicity according to our rhythmicity criteria. Chi-Square analysis revealed that of 144 total control NPCs screened, 25 (17.4%) were rhythmic, along with 22/86 (25.5%) of BD Li Responder and 8/73 (10.9%) of BD Li Non-Responder cells. This suggests a trend of arrythmicity in BD Li-NR cells compared to Control and BD Li-R cells. Out of the cells that did display rhythmicity, BD cells had significantly reduced Fast Fourier Transform (FFT) values, or weaker circadian rhythms, compared to control subject-derived cells (Control: 0.2433 ± 0.014, BD: 0.2066 ± 0.012, $p = 0.047$; **Figure 3.5A)**.

Cells that passed initial rhythmicity criteria were next analyzed for phase alignment. Circadian phase values were converted to polar coordinates, then plotted on a 360° polar graph corresponding to 24-hour cycle **(Figure 3.5B)**. Rayleigh's test, which evaluates the distribution

of points on a circle, found significant clustering in control cell phase values but not in either BD diagnosis group (Control: $p = 0.013$, BD Li-R: $p = 0.965$, BD Li-NR: $p = 0.241$). So few BD Li-NR cells were rhythmic that the apparent clustering was deemed likely to occur by chance and not statistically significant. More single cell recordings will be needed to determine the degree of phase alignment in each diagnosis group. The current analyses indicate that BD Li-NR cells are less likely to display circadian rhythms than BD Li-R or control subject cells, and of the cells that are rhythmic, rhythm phase appears to vary randomly. BD Li-R cells are more likely to display circadian rhythms, but do not show significant phase-alignment.

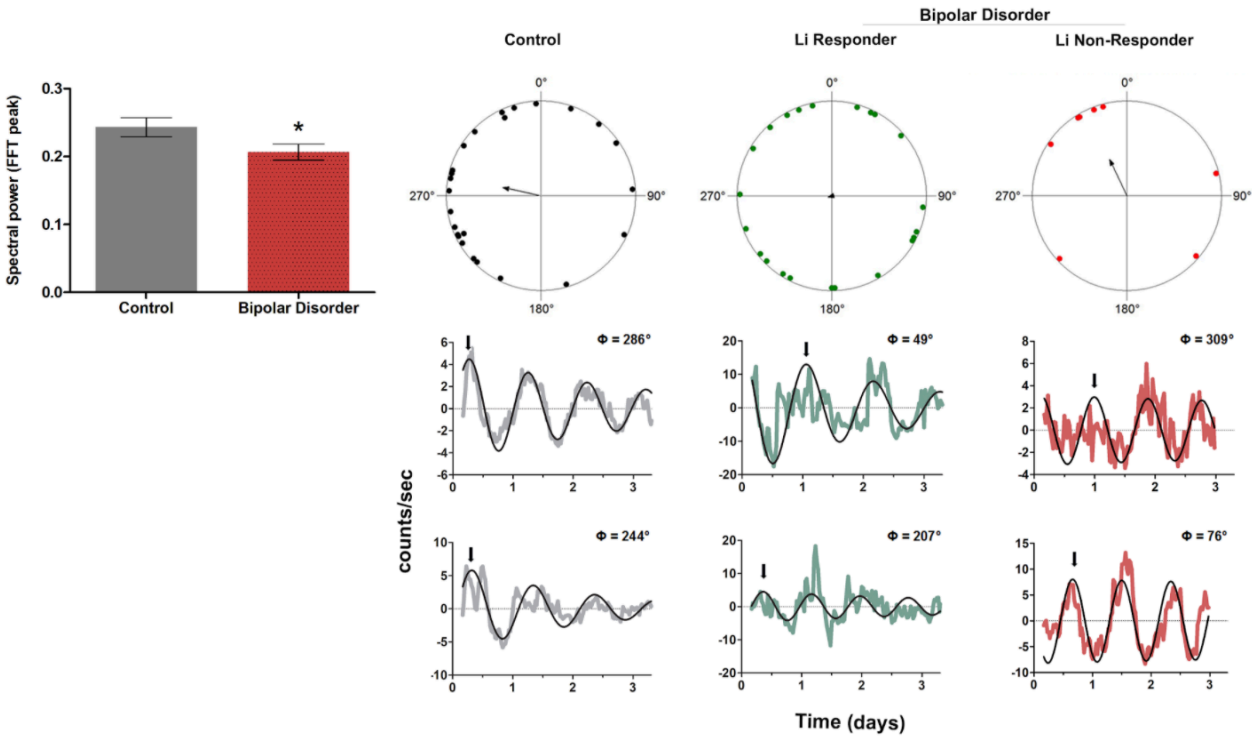

Figure 3.5: Single cell analysis reveals that BD NPCs are less rhythmic and less phase-aligned compared to Control NPCs. NPCs were transduced with a *Per2-luc* lentiviral reporter and a bioluminescence microscope was used to record bioluminescence over a 5-day period. **(A)** Fast Fourier Transform (FFT) peak comparison. For each cell analyzed that passed an initial criteria for rhythmicity (rhythm period 18-28 hours, FFT > 0.15), cell FFT values were pooled by diagnosis group, with BD Li-R and BD Li-NR data combined (Control = 0.2433 ± 0.014, BD = 0.2066 ± 0.012). Two-tailed, unpaired T Test revealed a significant difference between Control and BD average FFT values ($p < 0.047$). **(B, top panel)** Polar coordinate graphs of **(left)** Control, **(center)** BD Li Responder and **(right)** BD Li Non-Responder NPC phase. For each cell analyzed that passed initial criteria for rhythmicity, cell circadian phase was calculated and charted as an individual dot. Rayleigh's analysis revealed a significant clustering in Control cell phase values ($p = 0.013$). BD Li-NR cells did not pass the initial rhythmicity criteria in sufficient numbers to yield an analyzable range of phase values, but the present phase values appear to be widely scattered. **(B, bottom panel)** Representative traces from two cells each of **(left)** Control, **(center)** BD Li-R and **(right)** BD Li-NR NPCs, illustrating the proposed rhythm phase alignment in each diagnosis group. The colored lines indicate the bioluminescence emitted by a single cell within a 35mM dish of cells plated at 90 x 10^3 cells/well, and the black line indicates the best-fit damped sine curve generated by the LumiCycle Analysis software. n=2 control subjects, 2 BD Li-R, and n=1 BD Li-NR cell lines, with 60-80 cells analyzed per cell line. Data analysis was conducted by Dr. Himanshu Mishra.

3.6 Temperature Entrainment Rescues Circadian Rhythm Amplitude and Period in BD Neurons

Human circadian rhythms are maintained on a daily basis by a specialized population of photoreceptive retinal ganglion cells that project to the suprachiasmatic nucleus, allowing our sleep/wake and activity cycles to align with external day/night cycles (Porcu et al., 2019). Therapies that use environmental cues to re-entrain circadian rhythms, such as Bright Light Therapy, have shown efficacy in reducing depressive symptoms in BD patients (Zhou et al., 2018). This suggests that BD patient circadian rhythms may respond inadequately to normal rhythm cues or may be sensitive to rhythm perturbances. Prior work in BD patient-derived fibroblasts has shown that temperature cycling can entrain cell molecular circadian rhythm to a 24-hour period, indicating that temperature entrainment may provide an *in vitro* model for *in vivo* external entrainment cues (Nudell et al., 2019).

In order to extend the previous work into neurons, we recorded *Per2-luc* rhythms in identically-prepared cell samples both at a constant 35°C condition and in a 35°C/37.5°C 12:12 alternating temperature cycle **(Figure 3.6A-F)**. The cells in the temperature entrainment condition had significantly increased rhythm amplitudes, although BD Li-NR rhythms remained relatively low-amplitude compared to control subject and BD Li-R rhythms **(Figure 3.6D)**. Two-way ANOVA revealed a significant effect of diagnosis ($p = 0.010$), temperature ($p < 0.0001$), and diagnosis x temperature interaction ($p = 0.048$). The damping constant, indicating the rate of amplitude decay, was also increased by temperature entrainment, although this effect was only significant in control and BD Li-R cells **(Figure 3.6E**). Two-way ANOVA revealed a significant effect of temperature ($p < 0.0001$) and diagnosis x temperature interaction ($p = 0.005$). Control and BD Li-R neurons had ~24 hour circadian periods in both constant

temperature and temperature entrainment conditions, but temperature entrainment caused a significant increase in BD Li NR rhythm period, bringing it closer to an adaptive 24-hour rhythm (CC = 23.32 ± 0.26 hr, C = 24.28 ± 0.07 hr, p = 0.005; **Figure 3.6F**).

These results validate our experimental model, indicating that hiPSC-derived cells are capable of surviving and producing *Per2-luc* fluorescent signals for up to 14 consecutive days of recording. As such, the rhythm damping usually observed after 5 days of recording in constant conditions **(Figure 3.3, 3.4)** may be due to cells falling out of phase with one another, as suggested in Welsh et al., 2004. The addition of an external entrainment factor forces cells within a population to remain in phase, lessening destructive interference and generating a greater rhythm amplitude and slower damping. However, the effects of temperature entrainment appear to be blunted in BD Li Non-Responder cells, indicating that phase differences in BD Li Non-Responder cell rhythms may be less responsive to external entrainment cues.

Figure 3.6: Temperature entrainment rescues circadian rhythm amplitude and period and lessens rhythm damping in BD neurons. Neurons were transduced with a *Per2-luc* lentiviral reporter and a luminometer was used to record bioluminescence over a 14-day period. (**A-C)** Representative traces from **(A)** Control, **(B)** BD Li Responder and **(C)** BD Li Non-Responder neurons. The gold line indicates the bioluminescence emitted by a single 35mM dish of cells plated at 250 x 10^3 cells/well and maintained at 35°C during recording, and the overlayed black line indicates the best-fit damped sine curve generated by the LumiCycle Analysis software. The "Temp Condition" colored line indicates the bioluminescence emitted by an identically-prepared 35mM dish of cells subjected to a 35°C/37.5°C 12:12 alternating temperature cycle during recording. The same three lines (n=1 control, 1 BD Li-R, 1 BD Li-NR) were recorded in triplicate in both the "Temperature Condition" and "Control Condition" during each of two separate experimental trials. **(D)** Average circadian rhythm amplitude. For each cell line, the average rhythm amplitude across all trials was calculated in both conditions (Constant Condition: Control = 4.304 ± 0.221 counts/sec, BD Li-R = 3.668 ± 0.995 counts/sec, BD Li-NR = 0.791 ± 0.060 counts/sec; Temperature Cycling Condition: Control = 27.05 ± 6.729 counts/sec, BD Li-R = 22.78 ± 2.922 counts/sec, BD Li NR = 11.14 ± 1.314 counts/sec). Two-way ANOVA revealed a significant effect of diagnosis ($p = 0.0103$), temperature ($p < 0.0001$) and diagnosis x temperature interaction ($p = 0.0482$). **(E)** Average circadian rhythm damping constant. For each cell line, the average rhythm damping constant across all trials was calculated in both conditions (Constant Condition: Control = 1.842 ± 0.172 days, BD Li-R = 2.802 ± 0.315 days, BD Li-NR = 4.402 ± 0.406 days; Temperature Cycling Condition: Control = 8.904 ± 1.048 days, BD Li-R = 6.735 ± 1.179 days, BD Li NR = 5.873 ± 0.679 days). Two-way ANOVA revealed a significant effect of temperature ($p < 0.0001$) and diagnosis x temperature interaction ($p = 0.0048$). **(F)** Average circadian rhythm period. For each cell line, the average rhythm period across all trials was calculated in both conditions (Constant Condition: Control = 23.98 ± 0.085 hr, BD Li-R = 24.08 ± 0.147 hr, BD Li-NR = 23.32 ± 0.256 hr; Temperature Cycling Condition: Control = 24.03 ± 0.075 hr, BD Li-R = 24.17 ± 0.061 hr, BD Li NR = 24.28 ± 0.075 hr). Two-tailed, unpaired T Test revealed a significant difference between Constant Condition and Temperature Condition period in BD Li-NR ($p = 0.0047$).

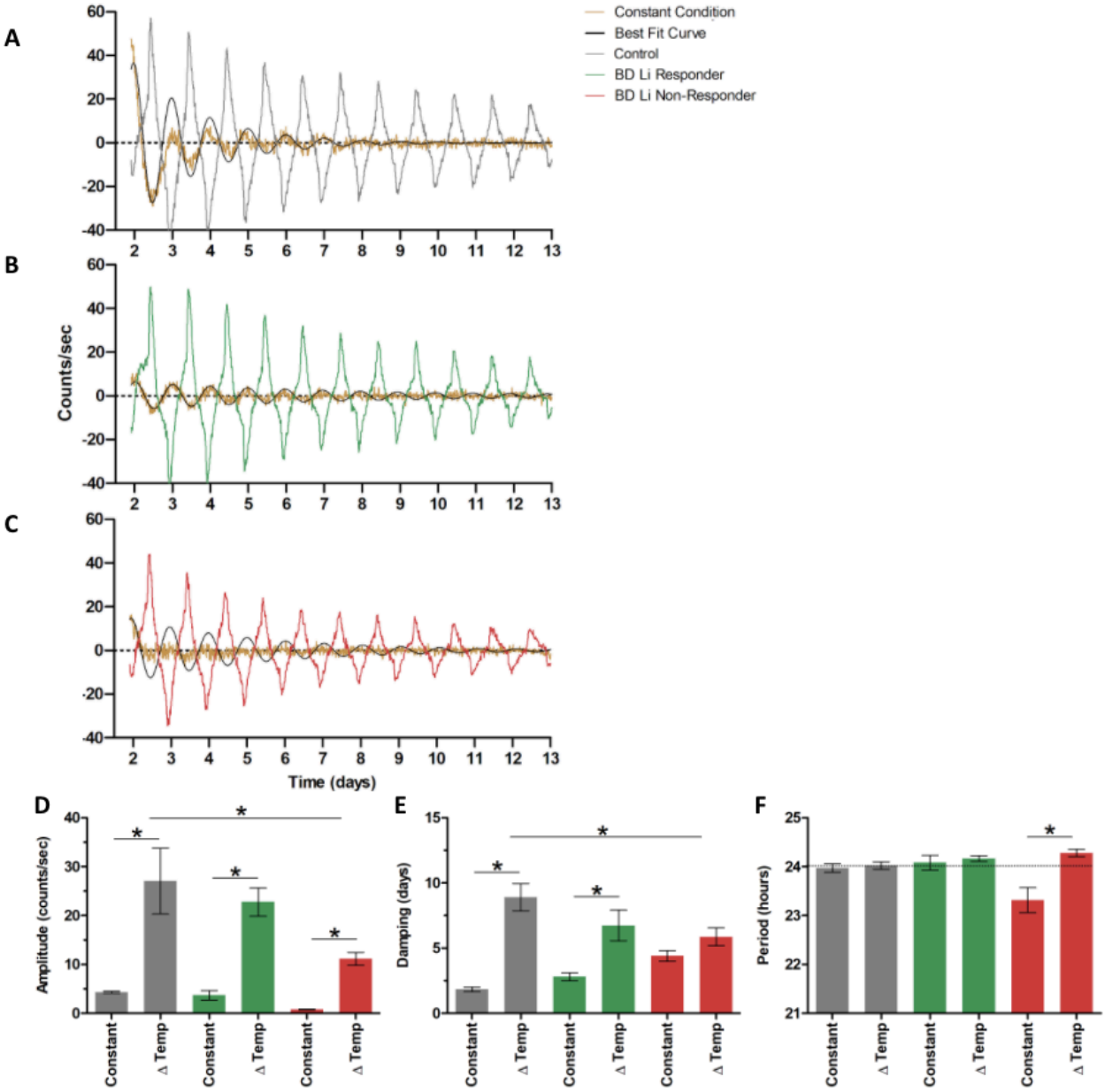
A
B
C
D
E
F
Constant Condition
Best Fit Curve
Control
BD Li Responder
BD Li Non-Responder
Counts/sec
Time (days)
Amplitude (counts/sec)
Damping (days)
Period (hours)
Constant
Δ Temp

Figure 3.6

DISCUSSION

Summary of Findings

Our characterization of hiPSC-derived NPCs and glutamatergic neurons indicates that BD-associated dysregulation of the molecular circadian clock begins during neuronal development, in the NPC stage (Figure 3.2, 3.3). Key aspects of BD symptomology, such as Lithium response or non-response, are similarly mirrored in NPC rhythm phenotypes (Figure 3.3). In differentiated neurons, BD Li Non-Responder-derived cells were, as expected, found to have circadian rhythms that were not modulated by lithium treatment (Figure 3.4), and were also found to be more phase-dispersed (Figure 3.5) and more resistant to external entrainment factors than were BD Li Responder cells and healthy control cells (Figure 3.6). In BD Li Responder and healthy control neurons, we observed concentration-dependent circadian rhythm lengthening in response to lithium, in agreement with clinical whole-human data (Johnsson et al., 1983) and based on previous rhythm entrainment studies in fibroblasts (Nudell et al., 2019) developed a heat-entrainment protocol that successfully induced high-amplitude, 24-hour circadian rhythms in neurons from all diagnosis groups (Figure 3.6). Further characterization of the molecular circadian rhythms of BD patient-derived neurons has the potential to reveal clinically-relevant indicators of BD lithium response.

The hiPSC-derived Neuron Model of BD

Previous clinical studies have found that in several areas of the brain, such as the prefrontal cortex and cingulate gyrus, glutamate levels are elevated in BD patients (Jun et al., 2014). Furthermore, normalized levels of glutamate were associated with response to mood stabilizing medication and disease remission, indicating that glutamatergic signalling is disturbed

in BD patients and may play a key role in BD symptomology (Jun et al., 2014). Using fibroblasts donated by patients already well-characterized in a clinical context, we successfully generated hiPSC-derived cortex-like glutamatergic neurons. Cell identity was confirmed via immunocytochemistry (Figure 3.1). This model may more accurately reflect the molecular conditions present in BD than did previous models, such as fibroblasts, which do not form synaptic connections, exhibit electrical activity, or express glutamate or other neurotransmitters which may be vital to BD etiology.

While our innovative experiments were successful in many ways, there are shortcomings of the hiPSC-derived neuron model and aspects that may be improved in future experiments. For example, hiPSC are costly to maintain and the differentiation process is time-consuming, leading to small samples sizes despite the widespread availability of skin or blood cell samples from eligible patients. Furthermore, a mixed neuron sample with an even longer maturation period, as provided by neuronal organoids, may be a more accurate representation of the human brain (Trujillo et al., 2019). Organoids can be grown to contain populations of both glutamatergic and GABAergic neurons, potentially modelling embryonic neural circuitry, and have been found to recreate synchronized firing patterns reminiscent of those found in pre-term fetuses (Trujillo et al., 2019). However, even current organoid models struggle to capture the complex interdependence between different brain regions and, like 2-D cultures, cannot respond to light, one of the most important entrainment factors in whole-organism circadian rhythm regulation (Trujillo et al., 2019). In order to understand the contribution of different cell types to BD molecular circadian rhythms, the McCarthy lab aims to generate hiPSC-derived GABAergic and dopaminergic neurons and further examine cell morphology and the interaction between various GWAS-identified risk genes for BD and the molecular clock. We are also preparing to conduct

electrophysiology analyses using multi-electrode arrays, to determine the extent to which action potential firing is synchronized in BD vs. control neuronal cultures, and if it is potentially under circadian control.

Circadian rhythms in hiPSC-derived NPCs and Neurons

Our model allowed us to expand upon circadian rhythm experiments previously conducted in fibroblasts using a model that more closely approximated the BD patient brain, in the process confirming circadian rhythm abnormalities, such as differences in rhythm period, seen in fibroblasts (McCarthy et al., 2013). The hiPSC model of BD also allowed us to maintain cell lines in the NPC and neuron stages, permitting investigation into the developmental trajectory of BD previously impossible in mature fibroblast cells. This allowed us to identify differences in BD cell gene expression (Figure 3.2) and circadian rhythms (Figure 3.3) in the progenitor cell stage, supporting the idea that BD has origins in prenatal development (O'Shea et al., 2016).

Moreover, circadian rhythm abnormalities present in the NPCs stage appeared to persist or even amplify during maturation. Gene expression analysis indicated that in BD NPCs only negative transcriptional regulators *PER2* and *CRY1* were dysregulated, while in neurons both positive and negative components of the TTFL were affected (*PER2, CRY1,* and *BMAL1*; Figure 3.2). Similarly, luminometry revealed that the BD Li-NR low rhythm amplitude phenotype was present in both NPCs and neurons (Figure 3.3). Cells from both BD diagnosis groups had a short period relative to healthy controls, but this trend was significant only in the NPC stage (Figure 3.3). There was a smaller difference in rhythm period between control and BD neurons, possibly indicating that as BD neurons mature, initial abnormalities in circadian period regulation may be

partially, but not completely, corrected towards a more adaptive ~24-hour period. Failure to develop an appropriately-regulated molecular circadian period, and the resulting mis-alignment with external circadian entrainment factors such as sunlight, may contribute to clinically observed rhythm irregularities in patients with BD.

Single Cell Analysis and Rhythm Entrainment in BD Li Non-Responders

Low rhythm amplitude, found in BD Li Non-Responder NPC and neurons, is likely due to two major factors. First, lower overall expression of circadian rhythms in individual cells as demonstrated by low spectral power estimates (Figure 3.5A). Second, there was greater phase dispersion in these cell populations (Figure 3.5B). Welsh et al. found that as cells within a culture continue to generate autonomous circadian rhythms but gradually fall out of phase with one another, the destructive interference from the asynchronous bioluminescent signals result in rapidly-damping, low amplitude population-level rhythms (Welsh et al., 2004, 2010). We found that BD Li Non-Responder cells were resistant to external clock-modifying or clock-entraining factors, as seen in an expected failure to respond to lithium treatment while BD Li Responder and control cells exhibited lithium concentration-dependent period lengthening (Figure 3.4), and a reduced temperature entrainment-mediated increase in rhythm amplitude and damping constant relative to the other groups (Figure 3.6). Combined with the greater phase dispersal in BD Li Non-Responder cells directly observed via single cell analysis (Figure 3.5), and the roughly 10-fold increase in BD Li Non-Responder rhythm amplitude when cells were synchronized via temperature entrainment (Figure 3.6), these results suggest that BD Li Non-Responder cell populations may express “low-amplitude rhythms” not simply because of weak clock gene expression in each cell but also because of greater phase dispersion. Clinical lithium non-

response may be associated with a fundamentally different circadian dysregulation than is found in BD Li Responders, as cells derived from the latter group express a circadian clock that can be modulated via external cues, while BD Li Non-Responder cells have a blunted or absent response to those same cues.

However, as shown by the amplitude increase and period correction in temperature-entrained conditions, BD Li Non-Responder cells still contain the core clock machinery necessary to express robust, 24-hour circadian rhythms. Further investigation will be needed to elucidate the mechanism through which temperature entrainment affects molecular circadian rhythms, but these findings indicate that the BD Li Non-Responder circadian phenotype may be salvageable. We speculate that the lack of neuronal synchrony and poor ability to entrain circadian rhythms to external cues may contribute to the clinically-observed disordered sleep/wake, mood, and activity cycles in BD Li Non-Responder patients, even when treated with lithium. Bright Light Therapy, which recreates exposure to strong natural sunlight, has shown efficacy in treating acute BD depression without inducing mania (Zhou et al., 2018); with further study, BLT and other rhythm entrainment-focused therapies and pharmacotherapies may be able to ameliorate circadian dysregulation in BD Li Non-Responder patients.

The development and characterization of this patient fibroblast-derived hiPSC model of BD enables further research into circadian rhythm dysregulation in BD, while providing a human cell model for rapid pharmacological testing and drug discovery. Future research may contribute to the development of an *in vitro* drug screening process that could determine lithium response profile based on a patient skin sample. Such a personalized medicine approach to pharmacotherapy has the potential to reduce the significant cost and time associated with current trial-and-error prescription methods, thereby improving quality of life for BD patients.

REFERENCES

Beyer, D. K. E., & Freund, N. (2017). Animal models for bipolar disorder: from bedside to the cage. *International Journal of Bipolar Disorders,* 5(1). doi:10.1186/s40345-017-0104-6

Brennand, K. J., Simone, A., Tran, N., & Gage, F. H. (2012). Modelling psychiatric disorders at the cellular and network levels. *Molecular Psychiatry*, 17(12): 1239-1253. doi:10.1038/mp.2012.20

Clemente A. S., Diniz, B. S., Nicolato, R., Kapczinski, F. P., Soares, J. C., Firmo, J. O., Castro-Costa, E. (2015). Bipolar disorder prevalence: a systematic review and meta-analysis of the literature. *Brazilian Journal of Psychiatry,* 37(2). doi:10.1590/1516-4446-2012-1693

Culpepper L. (2014). The diagnosis and treatment of bipolar disorder: decision-making in primary care. *The primary care companion for CNS disorders*, *16*(3), PCC.13r01609. doi:10.4088/PCC.13r01609

Grof P, Duffy A, Cavazzoni P, Grof E, Garnham J, MacDougall M, O'Donovan C., Alda M. (2002). Is response to prophylactic lithium a familial trait? *J Clin Psychiatry* 63:942–7.

Hirota, T., Lewis, W. G., Liu, A. C., Lee, J. W., Schultz, P. G., & Kay, S. A. (2008). A chemical biology approach reveals period shortening of the mammalian circadian clock by specific inhibition of GSK-3beta. *Proceedings of the National Academy of Sciences of the United States of America*, *105*(52), 20746–20751. doi:10.1073/pnas.0811410106

Johnsson, A, Engelmann, W, Pflug, B, Klemke, W (1983) Period lengthening of human circadian rhythms by lithium carbonate, a prophylactic for depressive disorders. Int J Chronobiol 8:129-147.

Jun et al, 2014 : Jun, C., Choi, Y., Lim, S. M., Bae, S., Hong, Y. S., Kim, J. E., Lyoo, I. K. (2014). Disturbance of the Glutamatergic System in Mood Disorders. Experimental Neurobiology 23 (1): 28-35. https://doi.org/10.5607/en.2014.23.1.28

Kaladchibachi, S. A., Doble, B., Anthopoulos, N., Woodgett, J. R., Manoukian, A. S. (2007). Glycogen synthase kinase 3, circadian rhythms, and bipolar disorder: a molecular link in the therapeutic action of lithium. *Journal of circadian rhythms*, *5*, 3. doi:10.1186/1740-3391-5-3

Klein, P. S., Melton, D. A. (1996). A molecular mechanism for the effect of lithium on development. *Proceedings of the National Academy of Sciences of the United States of America*, *93*(16), 8455–8459. doi:10.1073/pnas.93.16.8455

Landgraf, D., Long, J. E., Proulx, C. D., Barandas, R., Malinow, R., & Welsh, D. K. (2016). Genetic Disruption of Circadian Rhythms in the Suprachiasmatic Nucleus Causes Helplessness, Behavioral Despair, and Anxiety-like Behavior in Mice. *Biological psychiatry*, *80*(11), 827–835. https://doi.org/10.1016/j.biopsych.2016.03.1050

Luis, A. R. R., McCarthy, M. J., Mishra, H. K., Wei, H. (2019). Gene Expression Analysis of Circadian Clock Genes in a Human Stem Cell-Derived Neuronal Model of Bipolar Disorder. Thesis for a Master of Science in Biology at UC San Diego.

Machado-Vieria, R., Manji, H. K., Zarate, C. A. (2009). The role of lithium in the treatment of bipolar disorder: converging evidence for neurotrophic effects as a unifying hypothesis. *Bipolar Disorder*, 11(Suppl 2): 92-109. doi:10.1111/j.1399-5618.2009.00714.x.

McCarthy, M., Wei, H., Marnoy, Z., Darvish R. M., McPhie D. L., Cohen B. M., Welsh D. K. (2013). Genetic and clinical factors predict lithium's effects on PER2 gene expression rhythms in cells from bipolar disorder patients. *Transl Psychiatry* **3,** e318. doi:10.1038/tp.2013.90

McCarthy, M. J., Wei, H., Nievergelt, C. M., Stautland, A., Maihofer, A. X., Welsh, D. K., Shilling, P., Alda, M., Alliey-Rodriguez, N., Anand, A., Andreasson, O. A., Balaraman, Y., Berrettini, W. H., Bertram, H., Brennand, K. J., Calabrese, J. R., Calkin, C. V., Claasen, A., Conroy, C., Coryell, W. H., Craig, D.W., D'Arcangelo, N., Demodena, A., Djurovic, S., Feeder, S., Fisher, C., Frazier, N., Frye, M. A., Gage, FH., Gao, K., Garnham, J., Gershon, ES., Glazer, K., Goes, F., Goto, T., Harrington, G., Jakobsen, P., Kamali, M., Karberg, E., Kelly, M., Leckband, S. G., Lohoff, F., McInnis, M. G., Mondimore, F., Morken, G., Nurnberger, J. I., Obral, S., Oedegaard, K. J., Ortiz, A., Ritchey, M., Ryan, K., Schinagle, M., Schoeyen, H., Schwebel, C., Shaw, M., Shekhtman, T., Slaney, C., Stapp, E., Szelinger, S., Tarwater, B., Zandi, P. P., Kelsoe, J. R. (2019). Chronotype and cellular circadian rhythms predict the clinical response to lithium maintenance treatment in patients with bipolar disorder. *Neuropsychopharmacology : official publication of the American College of Neuropsychopharmacology*, *44*(3), 620–628. doi:10.1038/s41386-018-0273-8

McCarthy M. J. (2019). Missing a beat: assessment of circadian rhythm abnormalities in bipolar disorder in the genomic era. *Psychiatric genetics*, *29*(2), 29–36. https://doi.org/10.1097/YPG.0000000000000215

McGuffin, P., Rijsdijk, F., Andrew, M., Sham, P., Katz, R., & Cardno, A. (2003). The heritability of bipolar affective disorder and the genetic relationship to unipolar depression. *Archives of general psychiatry*, *60*(5), 497–502. https://doi.org/10.1001/archpsyc.60.5.497

Merikangas K. R., Jin R., He J-P, Kessler R. C., Lee S., Sampson N. A., Viana M. C., Andrade L. H., Hu C., Karam E. G., Ladea M., Medina-Mora M. E., Ono Y., Posada-Villa J., Sagar R., Wells J. E., Zarkov Z. (2011). Prevalence and correlates of bipolar spectrum disorder in the world mental health survey initiative. *Arch Gen Psychiatry* 68(3):241-251. doi:10.1001/archgenpsychiatry.2011.12

Mertens, J., Want, Q. W., Kim, Y., Yu, D. X., Pham, S., Yang, B., Zheng, Y., Diffenderfer, K. E., Zhang, J., Soltani, S., Eames, T., Schafer, S. T., Boyer, L., Marchetto, M. C., Nurnberger, J. I., Calabrese, J. R., Oedegaard, K. J., McCarthy, M. J., Zandi, P. P., Alda, M., Nievergelt, C. M., The Pharmacogenomics of Bipolar Study, Mi, S., Brennand, K. J., Kelsoe, J. R., Gage, F. H., Yao, J. (2015). Differential responses to lithium in hyperexcitable neurons from patients with bipolar disorder. *Nature*, *527*(7576), 95–99. https://doi.org/10.1038/nature15526

Nudell, V., Wei, H., Nievergelt, C., Maihofer, A. X., Shilling, P., Alda, M., Berrettini, W. H., Brennand, K. J., Calabrese, J. R., Coryell, W. H., Covault, J. M., Frye, M. A., Gage, F., Gershon, E., McInnis, M. G., Nurnberger, J. I., Oedegaard, K. J., Shekhtman, T., Zandi, P. P., Kelsoe, J. R., McCarthy, M. J. (2019). Entrainment of Circadian Rhythms to Temperature Reveals Amplitude Deficits in Fibroblasts from Patients with Bipolar Disorder and Possible Links to Calcium Channels. *Molecular neuropsychiatry*, *5*(2), 115–124. https://doi.org/10.1159/000497354

Oedegaard, K. J., Alda, M., Anand, A., Andreassen, O. A., Balaraman, Y., Berrettini, W. H., Bhattacharjee, A., Brennand, K. J., Burdick, K. E., Calabrese, J. R., Calkin, C. V., Claasen, A., Coryell, W. H., Craig, D., DeModena, A., Frye, M., Gage, F. H., Gao, K., Garnham, J., Gershon, E., Jakobsen, P., Leckband S. G., McCarthy M. J., McInnis M. G., Maihofer A. X., Mertens J., Morken G., Nievergelt C. M., Nurnberger, J., Pham, S., Schoeyen, H., Shekhtman, T., Shilling, P. D., Szelinger, S., Tarwater, B., Yao, J., Zandi, P. P., Kelsoe, J. R. (2016). The Pharmacogenomics of Bipolar Disorder study (PGBD): identification of genes for lithium response in a prospective sample. *BMC psychiatry*, *16*, 129. https://doi.org/10.1186/s12888-016-0732-x

O'Shea, S. K. & McInnis, M. G. Neurodevelopmental origins of bipolar disorder: iPSC models. (2016). *Molecular and Cellular Neuroscience,* 73(1), 63-83. doi:10.1016/j.mcn.2015.11.006

Porcu, A., Gonzalez, R. & McCarthy, M.J. (2019). Pharmacological Manipulation of the Circadian Clock: A Possible Approach to the Management of Bipolar Disorder. CNS Drugs 33: 981. doi:10.1007/s40263-019-00673-9

Roybal, K., Theobold, D., Graham, A., DiNieri, J. A., Russo, S. J., Krishnan, V., Chakravarty, S., Peevey, J., Oehrlein N., Birnbaum S., Vitaterna M. H., Orsulak, P., Takahashi J. S., Nestler E. J., Carlezon W. A. Jr., McClung, C. A. (2007). Mania-like behavior induced by disruption of CLOCK. *Proceedings of the National Academy of Sciences of the United States of America*, *104*(15), 6406–6411. doi:10.1073/pnas.0609625104

Trujillo C. A., Gao R., Negraes P. D., Gu J., Buchanan J., Preissl S., Wang A., Wu W., Haddad G. G., Chaim I. A., Domissy A., Vandenberghe M., Devor A., Yeo G. W., Voytek B., Muotri A. R. (2019). Complex oscillatory waves emerging from cortical organoids model early human brain network development. *Cell Stem Cell* 25, 558.e7–569.e7. doi:10.1016/j.stem.2019.08.002

Takahashi, K., Hong, H. K., Ko, C. H., McDearmon, E. L. (2008). The genetics of mammalian circadian order and disorder: implications for physiology and disease. *Nature Reviews Genetics,* 9(10), 764-775. doi:10.1038/nrg2430

Viswanath, B., Jose, S. P., Squassina, A., Thirthalli, J, Purushottam, M., Mukherjee, O., Vladimirov V., Patrinos G. P., Del Zompo M., Jain, S. (2015). Cellular Models to Study bipolar disorder: A systematic review. *Journal of Affective Disorders,* 184, 36-50. doi:10.1016/j.jad.2015.05.037

Welsh, D. K., Yoo, S. H., Liu, A. C., Takahashi, J. S., & Kay, S. A. (2004). Bioluminescence imaging of individual fibroblasts reveals persistent, independently phased circadian rhythms of clock gene expression. *Current biology: CB*, *14*(24), 2289–2295. https://doi.org/10.1016/j.cub.2004.11.057

Welsh, D. K., Takahashi, J. S., & Kay, S. A. (2010). Suprachiasmatic nucleus: cell autonomy and network properties. *Annual review of physiology*, *72*, 551–577. https://doi.org/10.1146/annurev-physiol-021909-135919

Zhou, T. H., Dang, W. M., Ma, Y. T., Hu, C. Q., Wang, N., Zhang, G. Y., Wang, G., Shi, C., Zhang, H., Guo, G., Zhou, S. Z., Feng, L., Geng, X., Tong, Y. Z., Tang, G. W., He, Z. K., Zhen, L., Yu, X. (2018). Clinical efficacy, onset time and safety of bright light therapy in acute bipolar depression as an adjuctive therapy: A randomized controlled trial. *Journal of Affective Disorders,* 227, 90-96. https://doi.org/10.1016/j.jad.2017.09.038